Journal of Fluorine Chemistry 135 (2012) 315–322

Contents lists available at SciVerse ScienceDirect

Journal of Fluorine Chemistry

journal homepage: www.elsevier.com/locate/fluor

Lyotropic liquid crystal phases of lithium perfluorinated fatty acid salts in aqueous solutions and molecular dynamics study of the lamellar phase

Panfeng Long, Hui Yan, Xiaohui Guo, Jingcheng Hao *

Key Laboratory of Colloid and Interface Chemistry (Shandong University) and Key Laboratory of Special Functional Aggregated Materials, Ministry of Education, Jinan 250100, China

ARTICLE INFO

Article history:
Received 6 September 2011
Received in revised form 19 December 2011
Accepted 21 December 2011
Available online 29 December 2011

Keywords:
Lamellar lyotropic liquid crystals
Perfluorinated fatty acid salts
Molecular dynamics simulation
Phase transition

ABSTRACT

Anisotropic lyotropic liquid crystal (LLC) of lithium perfluorinated fatty acid salts with long fluorocarbon chains (PFL-Li and PFM-Li, denotes lithium perfluorolaurate and perfluoromyristate, respectively) were prepared in aqueous solutions, and characterized by a variety of techniques in detail. Results of small-angle X-ray scattering (SAXS) study indicate that PFL/M-Li molecules are arranged to form lamellar liquid crystal in water, which were determined by freeze-fracture transmission electron microscopy (FF-TEM) images. Differential scanning calorimetry (DSC) measurements showed that, with the increase of the concentration of lithium perfluorolauric (PFL-Li), the temperature-dependent transition of LLC phases to micelle phases increases. However, LLC phases of lithium perfluoromyristate (PFM-Li), which is not temperature-sensitive, can not be transferred to micelle solution below 100 °C. Based on the SAXS measurements, constant volume and temperature (NVT) molecular dynamics (MD) simulation have been carried out to investigate the mechanism for the formation of lamellar LLC phases and their properties.

1. Introduction

Because of their unique characteristics, fluorinated surfactants have attracted a special interest to further develop in the properties available in surfactant mixtures. Compared to their hydrogenated counterparts, fluorinated surfactants show much lower critical micellar concentrations [1], higher surface activities and Krafft points [2]. Based on the general geometrical considerations of the packing of molecules into distinct aggregate shapes [3], fluorocarbon surfactants can more easily form bilayers [4–6], because of a larger cross-section and a higher rigidity of the fluorocarbon chain – compared to an analogous hydrocarbon chain.

Fluorinated surfactants can form the same types of micelles as hydrocarbon surfactants [6,7]. Small angle neutron-scattering (SANS) [8], NMR [9] and cyclic voltammetry methods [10] were used to study the mixed micelles of fluorocarbon and hydrocarbon surfactants. Up to the present, many scientific reports on the micellization of perfluorocarboxylate salts have appeared in the literature, such as the high resolution phase diagram, concentration–temperature dependence of a size and a shape of micelles and a micelle size and shape by SAXS and SANS in the CsPFO(C_7F_{15}COOCs)/water system [11–13]. In addition, the charge and aggregation number were determined for micelles as a function of surfactant concentration by SANS in the NaPFO(C_7F_{15}COONa)/water binary system [14]. Thermodynamics of micelle formation was studied for the counterion effect on the micellization of perfluorononanoic acid salts in an aqueous solution [15]. Fluorocarbon amphiphiles can also self-assemble into various types of aggregates, such as vesicles [16,17], emulsions [18,19], and lyotropic liquid crystals [4,20,21], sometimes are present together with hydrocarbon surfactants. The formation and stability of lyotropic liquid crystal phases in aqueous solutions depend on a balance between attractive hydrophobic interaction and hydrophilic forces of the headgroups. Consequently, it is distinct that LLC phases formed from surfactants normally tend to become a lamellar-phase, especially for perfluorinated surfactants at rather high surfactant concentrations. As early as 1974, Tiddy et al. studied hexagonal, lamellar, and intermediate phases in perfluorooctanoate/octanol/water system [22]. Subsequently, they researched into the lyotropic liquid crystalline phases in the lithium perfluorooctanoate/water system at fairly high surfactant concentrations [23]. Fontell and Lindman established original phase diagrams for perfluorononanoic acid and its salts in water, which include liquid crystal phases [4]. Recently, nonionic fluorocarbon surfactant/water systems were investigated to understand its role in the phase transitions between liquid crystals and to compare hydrogenated and fluorinated systems [24,25].

The investigated fluorinated surfactants have been mostly the ones with chain lengths of less than 10 carbon atoms because of their high Krafft points, and reports on longer chained fluorinated surfactants have been infrequent. Generally, the formation of LLC

* Corresponding author. Tel.: +86 531 88366074; fax: +86 531 88564750.
E-mail address: jhao@sdu.edu.cn (J. Hao).

0022-1139/$ – see front matter © 2011 Elsevier B.V. All rights reserved.
doi:10.1016/j.jfluchem.2011.12.012

phase of fluorinated surfactants is at fairly high concentrations, which restrict their applications because of the high price of fluorinated surfactants. In this paper, we report the studies of lamellar LLC phases of lithium perfluorinated fatty acid salts with long chains in aqueous solutions at rather low surfactant concentrations and room temperature. Originally, our aim was to investigate the influence of temperature, chain lengths, different counterions and concentration of perfluorinated fatty acid salts to the formation and stability of LLC phases. For the purpose of exploring the process and mechanism of the lamellar phase formation, NVT molecular dynamics (MD) simulation was carried out. Until now, computer simulations have been extensively used to investigate the aggregation of surfactants in aqueous solutions [26–29]. However, reports on the studies of MD simulations to aggregation of fluorinated surfactant are rare [30], and the influence of different counter ions on the formation and stability of LLC phases of perfluorinated fatty acid salts is not yet understood. We hope this work should create a better understanding of bilayers of fluorinated surfactant compared to their hydrogenated counterparts.

2. Results and discussion

2.1. Phase behavior of perfluoro fatty acid salts

It is known that the Krafft points of perfluorinated surfactants are generally high, so that less than C7 or C8 carbon chain compounds may be used at room temperature [1,2]. However, Krafft points should also be affected by the types of counterions. As shown in Table 1, when equivalent amount of perfluorinated fatty acids (200 mmol L^{-1}) and relevant alkalis were mixed together at room temperature, one can observe that isotropic micelle soluotions were formed in PFO-Li, PFO-Na and PFO-Cs solutions, except for PFO-K, because of its high Krafft point (25.6 °C) [2]. However, with the increasing of fluorocarbon chain length, LLC phases were formed in PFL-Li, PFM-Li and PFD-Cs solutions, which were inspected between crossed polarizers. The LLC phases formed in PFL-Li, PFM-Li solutions could be stable even after several months, while the LLC phase formed in a PFD-Cs solution was unstable and deposition occurred just several days. Fontell and Lindman have studied cesium perfluorooctanoate and water mixed system and confirmed that a lamellar structure existed in this system by ^2H NMR measurements [4]. We extrapolated the formation of LLC phases of perfluorofatty acid salts having some connection with their chain length and counterions. Herein, we should make clear that the krafft point of PFL-Li is 24.5 °C and PFM-Li is 32.8 °C from our solubility tests. However, both samples of PFL-Li and PFM-Li are translucent solutions, which are also very stable at room temperature. The fluorocarbon chains of lithium perfluorocarboxylate salts may either be present in fluid state or in crystalline form in this system [31–34]. So, the krafft point tests indicate that the fluorinated alkyl chains of PFM-Li are "rigid" in the LLC phase, which means the LLC-phase would thus be in a metastable state in room temperature. The melting transition temperature of fluorocarbon chains of PFL-Li descends with the decreasing of chain length, which are in the fluid state at room temperature.

Table 1
Typical phase behavior of 200 mmol L^{-1} perfluorinated fatty acids and relevant alkalis mixed together at 70.0 ± 0.1 °C, then the samples were kept at 25.0 ± 0.1 °C for at least two weeks before their phase behavior was inspected. 'P' denotes precipitation and 'L_1' the isotropic micellar phase in the table.

Alkali (200 mmol L^{-1})	LiOH	NaOH	KOH	CsOH
$C_7F_{15}COOH$ (PFOA)	L_1	L_1	P	L_1
$C_9F_{19}COOH$ (PFDA)	L_1	P	P	(LLC)
$C_{11}F_{23}COOH$ (PFLA)	LLC	P	P	P
$C_{13}F_{27}COOH$ (PFMA)	LLC	P	P	P

2.2. SAXS and FF-TEM measurements

The structural information of LLC phases can be obtained by SAXS measurements. Fig. 1(a and b) shows the SAXS patterns of LLC phases of PFL-Li and PFM-Li samples with different concentrations. We can see similar scattering curves obtained, and typically three scattering peaks appear with relative positions of 1:2:3, which correspond to the 0 0 1, 0 0 2, and 0 0 3 planes of the lamellar structures. Unexpectedly, we can observe that when the concentration of PFL-Li reaches 300 mmol L^{-1}, other sets of scattering peaks were obtained as shown in Fig. 1a. From the enlarged view as shown in Fig. 1c, one can see two sets of scattering peaks accord with the ratio 1:2, indicating other lamellar structures. Herein, we consider higher level lamellar structures self-assembly from bilayers of surfactant molecules with the increasing of the concentration. One could doubt that the SAXS results can be affected by the presence of solid or gel microstructures coexisting with the LLC state. However, we also measured the XRD by comparing experiments of (PFL-Li/PFM-Li) crystals and LLC phases (500 mM), as shown in Fig. S1. One can easily see that no surfactant crystallites form in PFL-Li and PFM-Li solutions. The pattern of PFL-Li/PFM-Li powder shows a typical feature from a crystalline powder solid. However, the pattern of the LLC phase shows only a very weak peak and no trace of a crystalline peak at all, indicating that the LLC phase are close to the amorphous state.

The extracted structure parameters are listed in Fig. 1d. It is clear that the lattice spacings ($d = 2\pi/q$, calculated from the first peak position) of PFL-Li are all smaller than those of PFM-Li with the same concentration, which can be explained by the longer length of PFM-Li. The longer fluorocarbon chains of PFM-Li makes the bilayers more hydrophobic, so the surfactant molecules arrange more closely, which may lead to much wider water interlayer in the LLC phase. Otherwise, the lattice spacings are reduced with the increasing of concentration of the two surfactants. This is because more surfactant molecules make the lamellar LLC phases more crowded, resulting in a smaller lattice spacing.

To describe the structures in detail, in particular to measure the thicknesses of the fluorocarbon bilayers, it is necessary to determine the specific volume of the surfactant. This was carried out using pycnometer vials with the size of 10 cm^3. The measurements showed that the partial specific volume for PFL-Li and PFM-Li in LLC solutions are about 0.681 and 0.605 cm^3/g (υ_s). Knowing the specific volume of the fluorocarbon surfactants and of the water (υ_w = 1.00 cm^3/g) and the lattice spacings (d) from SAXS measurements, it is possible to calculate the thickness of the fluorocarbon surfactant bilayers (d_s) using

$$d_s = \frac{d}{1 + (\upsilon_w/\upsilon_s)(1 - \omega/\omega)}$$

The obtained thicknesses of the fluorocarbon surfactant bilayers are listed in Fig. 2. One can observe that the thicknesses of PFL-Li are all smaller than those of PFM-Li with the same concentration, which are the same case of the lattice spacings. Because of the disordered conformation of the fluorocarbon chains, the thicknesses of the surfactant bilayers are significantly smaller than that of a double layer of fully fluorocarbon chains (about 3.0 nm). The shrinkage of the bilayer thicknesses may be caused by an interdigitation of the fluorocarbon chains, which was approved by molecular dynamics simulations. In addition, the thickness of the fluorocarbon surfactant bilayers rises with the increase of the surfactant concentrations in both systems. The possibility is that

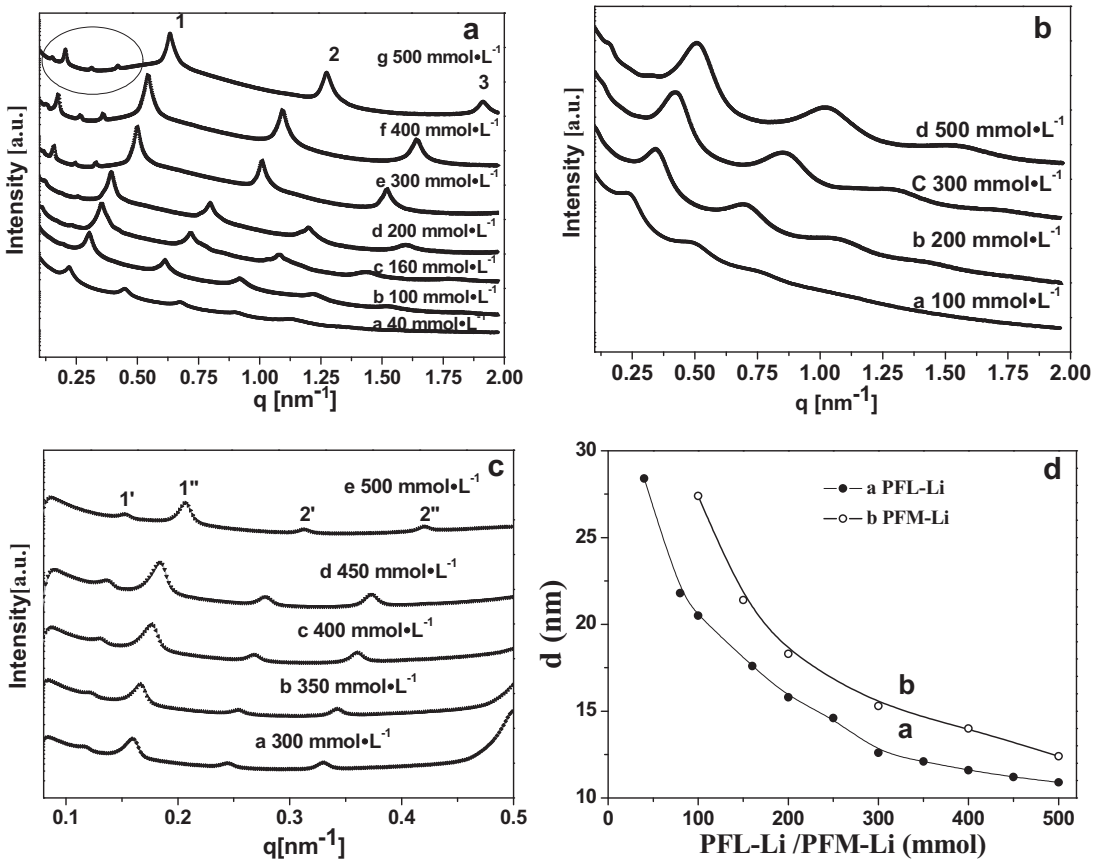

Fig. 1. SAXS scattering patterns of LLC phase samples with different concentrations (mmol L^{-1}) at 25.0 ± 0.1 °C: (a) PFL-Li in water; (b) PFM-Li in water; (c) an enlarged view of (a), including data of concentration of 350 and 450 mmol L^{-1}; (d) lattice spacings (d) varying with concentration of PFL-Li and PFM-Li in water.

the thermal oscillations of the chains have increased when water is added.

The lamellar structure of LLC phases of PFL-Li was further determined by FF-TEM measurements. The FF-TEM micrograph in Fig. 3 clearly show the lamellar structure of the hydrophobic bilayer and the water layer. It can be seen that the interlayers are heterogeneous, which are completely consistent with that obtained by the SAXS measurements. In addition, one can observe that interlayers with larger lattice spacings (larger than 10 nm from SAXS measurements) exist in the sample of 400 mM PFL-Li. It is interesting that the larger interlayer spacings are about 40 nm, which are about four times longer than that of dominating interlayer spacing. So, the FF-TEM images further demonstrates that our judgement about the higher level lamellar structures self-assembly from bilayers of surfactant molecules with the increasing of the concentration is reasonable.

2.3. DSC measurements of phase ttransition

It is necessary to note that the fluorocarbon alkyl chain has a great influence on the formation of LLC phases. We found that lithium perfluorooctanoate and lithium perfluorodecanoate cannot form LLC phase even when the concentration exceeds 500 mmol L^{-1}. Consequently, this observation could demonstrate

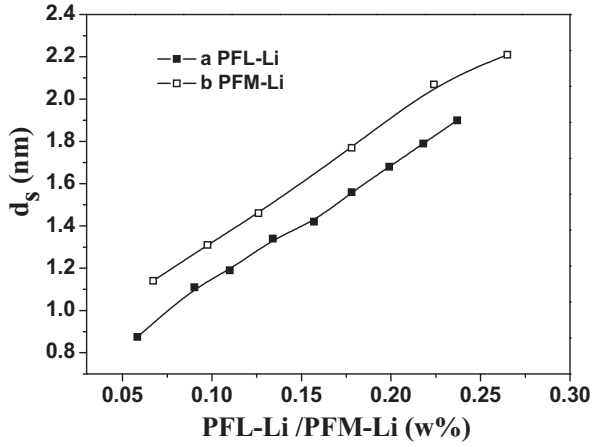

Fig. 2. Thicknesses of fluorocarbon chain bilayer (d_s) varing with mass fraction of PFL-Li and PFM-Li in water.

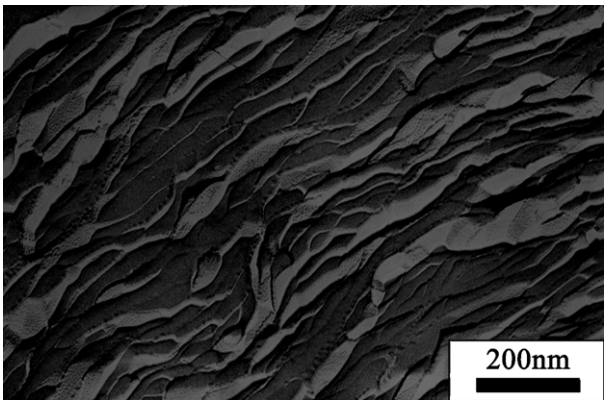

Fig. 3. Typical FF-TEM images of PFL-Li LLC phase sample with the concentration of 400 mmol L^{-1}.

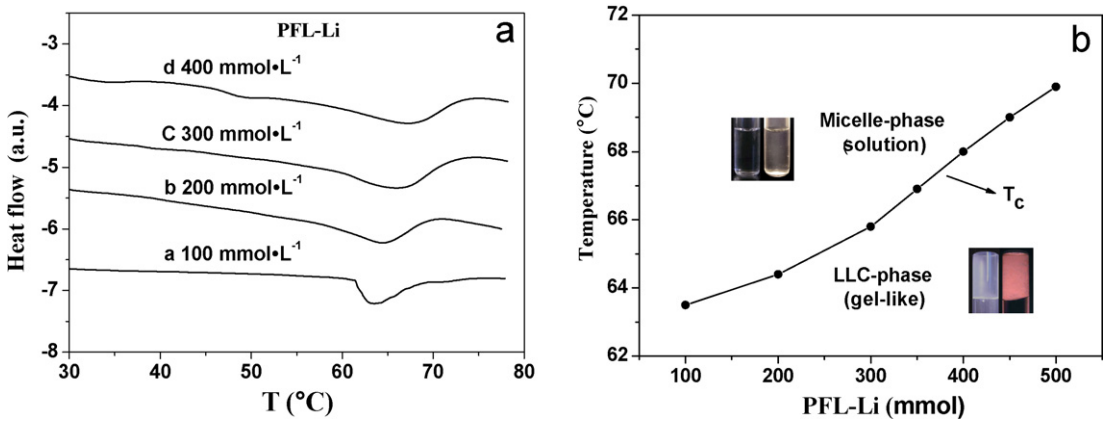

Fig. 4. (a) DSC data of LLC-phase samples with different concentrations in PFL-Li/water system; (b) part of phase diagram for PFL-Li in water, the transition temperature from gel-like to micellar solution against concentration of PFL-Li, the two inset photos are of representative micellar solution and gel-like samples, in the right side of samples with crossed polarizers.

that the hydrophobic interaction plays an important role in the formation of LLC phase. Because the lamellar structure of LLC phase is built by the noncovalent interaction, the formed LLCs of PFL-Li show thermal reversible gel-like to micellar solution transition. As shown in Fig. 4a, the increasing of concentration causes the higher transition temperature from the gel-like to micellar solution. The further influence of the concentration of PFL-Li on the transition temperature from gel-like to solution is shown in Fig. 4b, where the temperatures are plotted against the concentrations of PFL-Li. The transition temperature (T_c) from isotropic micellar phase to gel-like LLC phase rises with the increasing of PFL-Li concentration, which indicates that the interlayers of bilayer and water layer arrange more closely with the increasing of PFL-Li concentration. However, LLC-phases of PFM-Li, which show a considerable resistance against temperature rise, cannot transit to micelle solution below 100 °C. It can be seen that the stronger hydrophobic interaction with the increasing length of fluorocarbon chain keep the LLC phases in a thermal arrest. In previous work, Hoffmann and his coworkers have studied tetramethylammonium and ammonium salts of perfluorosurfactants show also a transition from the micellar solution to liquid crystal phase [35,36]. These systems show a nematic phase exists between the micellar solution and liquid crystal phase in the temperature range between 32 and 37 °C. The structure of the aligned sample that aligned and cooled down to 25 °C in a magnetic field was studied with small angle neutron scattering (SANS) at different temperatures.

As mentioned before, temperature and concentration of surfactant play an important role in the formation of LLC phase. In fact, Fig. 4b is a part of phase diagram for PFL-Li in water, the area above the plots is the isotropic micellar solution, and below the plots is the gel-like LLC-phase. According to the results of SAXS, DSC and optical microscopy measurements, the occurrence of LLC phase of PFL-Li solutions was confirmed at the region of 2.5–32.5 wt%.

2.4. Rheological properties of lamellar LLC-phase samples

Gel-like phases often have important and interesting rheological properties, which indicate their corresponding microcosmic structures [34,37,38]. The gel-like character of LLC samples is reflected in oscillatory rheology as shown in Fig. 5. Both samples show viscoelastic responses, however, there exhibit some differences. Over the range of 0.1–100 Hz, both the storage modulus (G′) and loss modulus (G″) rise with the increasing of frequency, and G′ is higher than G″ all along from Fig. 4a, indicating that the lamellar LLC phase of 200 mmol L^{-1} PFL-Li is highly viscoelastic. However, Fig. 4b shows, over the range of 0.1–100 Hz, both the storage modulus (G′) and loss modulus (G″) are nearly frequency-independent, and G′ is about one order magnitude higher than G″. The complex viscosity (η^*) of the samples linearly decreases with a slope of −1. Thus, the complex fluid behaves as a Bingham fluid, indicating that the sample of 200 mmol L^{-1} PFM-Li exhibits a gel-like response, also with highly viscoelastic properties.

To further explore the rheological behavior of lamellar LLC phases, steady-shear rheology of the samples with different concentrations of PFL-Li and PFM-Li was investigated. Typical steady-shear rheograms, i.e., apparent viscosity (η) as a function of shear rate for the lamellar LLC phase samples with different

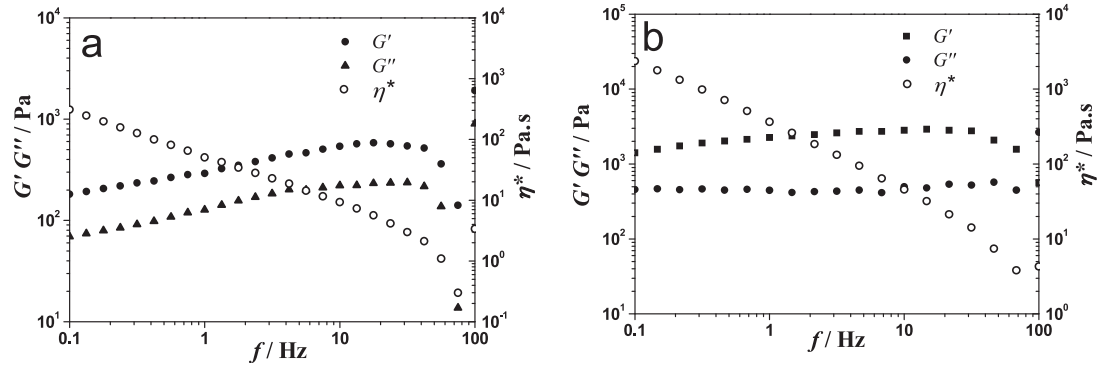

Fig. 5. Typical oscillatory rheogram of gel-like LLC phase samples at 25.0 ± 0.1 °C: 200 mmol L^{-1} PFL-Li (a); 200 mmol L^{-1} PFM-Li (b).

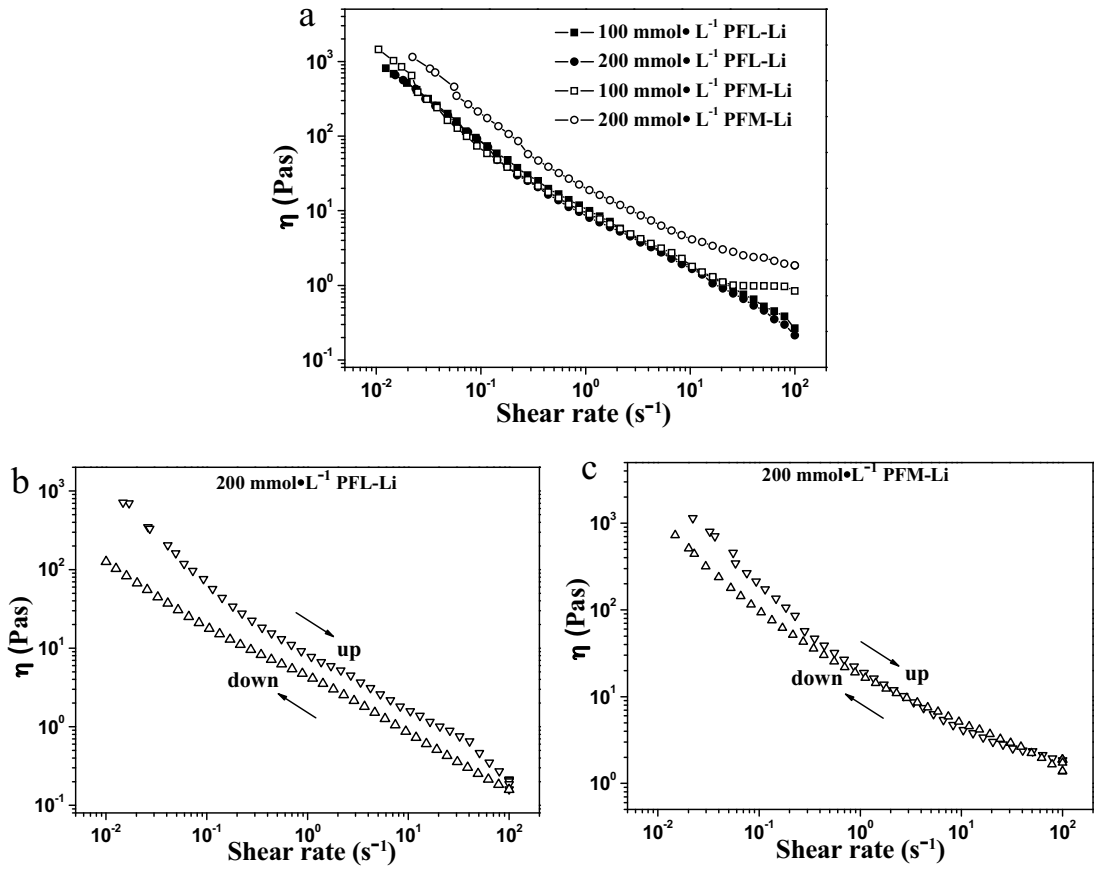

Fig. 6. Steady-shear rheological data for lamellar LLC phase samples with different concentrations of PFL-Li and PFM-Li (a); the hysteresis phenomenon for the samples of LLC phase for 200 mM PFL-Li (b) and for 200 mM PFM-Li at 25.0 ± 0.1 °C (c).

concentrations of PFL-Li and PFM-Li are shown in Fig. 6a. One can observe that all the samples show similar rheological behavior. The apparent viscosity, η, decreases remarkably with the increasing of shear rate, indicating a shear thinning behavior. This is because the lamellar structure of LLC phase is destroyed quickly with the increasing of the shear rates. Compared with the plot of the complex viscosity in oscillating measurements, the apparent viscosity values are about one order magnitude higher than those of the complex viscosity, when the shear rate values are the same as the absolute value of circular frequency for the two LLC phase samples of 200 mM PFL-Li and 200 mM PFM-Li. In many shear thinning liquids such plots are the same. This is known as the Cox–Merz-rule. Apparently, these LLC phase solutions of fluorocarbon surfactant systems do not follow the Cox–Merz-rule. This may be due to the complexity of the LLC phase solutions.

When the shear rate was increased first and then decreased, i.e., a cycle of shear rate variation was applied, a hysteresis loop is observed for the LLC phase sample of 200 mM PFL-Li, as shown in Fig. 6b. The shear viscosity in the down curve is lower than that in the up curve, suggesting that the destroyed structure did not recover back during the experimental time. However, in the case of the LLC phase sample of 200 mM PFM-Li, no hysteresis loop is observed, as shown in Fig. 6c. At high shear rate, the viscosity is generally the same in down and up curves, indicating that the lamellar structure has been destroyed absolutely. At low shear rate, the shear viscosity in the down curve is lower than that in the up curve, suggesting that the destroyed structure did not recover back during the experimental time. The stronger hydrophobic interaction with the increasing length of fluorocarbon chain in the LLC state increases the viscosity and viscoelasticity.

2.5. Molecular dynamics simulation

The MD simulation of different systems can be performed after charges and potentials are assigned to each of atoms or groups as shown in Fig. 7. The total energy is written as a combination of valence terms including diagonal and off-diagonal cross coupling terms, and nonbonded interaction terms, which include the Coulombic and Lennard–Jones functions for electrostatic and van der Waals interactions [39,40],

$$E = E_{\text{bonds}} + E_{\text{angles}} + E_{\text{dihedrals}} + E_{\text{cross}} + E_{\text{VDW}} + E_{\text{elec}} \quad (1)$$

where E_{VDW} and E_{elec} are given by Eq. (2):

$$E_{\text{non-bond}} = E_{\text{VDW}} + E_{\text{elec}} = \sum \varepsilon_{ij}\left[2\left(\frac{\sigma_{ij}}{r_{ij}}\right)^9 - 3\left(\frac{\sigma_{ij}}{r_{ij}}\right)^6\right] + \sum \frac{q_i q_j}{r_{ij}} \quad (2)$$

The COMPASS force field was used in the simulation [41,42].

According to the part of our experimental results and forerunners' predominant work [26,28,29], the initial configuration was constructed as follows: First, the initial lattice constants were chosen to give the surface area/molecule of 33 Å^2, and the height of the lattice was chose to give the lattice spacing of 160 Å, according to the results of SAXS measurements of 200 mmol L^{-1} PFL-Li LLC-phase sample. Second, a simulation box was set up by arranging a molecule bilayer of 50 PFL^- ions in the center and 50 Li^+ ions near the polar groups, according to the concentration of 200 mM PFL-Li LLC-phase sample. Finally, 1600 H_2O molecules were filled in the water box with the thickness of about 80 Å as shown in Fig. 7 (right), and this distance can avoid the effect of the

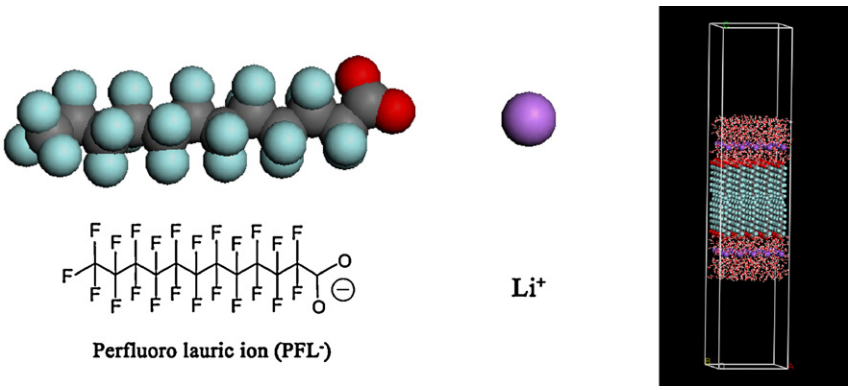

Fig. 7. Chemical structure illustration for perfluoro lauric ion (PFL^-) and Li^+. Color codes: bluish green, fluorine atoms; gray, carbon atoms; red, oxygen atoms; purple, lithium-ion (left); snapshot of the initial configuration (right). (For interpretation of the references to color in this figure legend, the reader is referred to the web version of this article.)

other boxes in the *z* direction due to the periodic boundary condition [40,43].

Simulation was carried out for bilayers made up of PFL^- with Li^- as counterions in aquous solution, using Materials Studio 5.0 molecular dynamics program package. The energies of the initial configuration were minimized with the Smart Minimizer method. After the minimization, the simulation was equilibrated at constant temperature and volume (NVT) for 2.0 ns with a time step of 1 fs. The results are analyzed from the coordinates which were saved every 10 ps.

Fig. 8 shows the snapshots of the configuration with four boxes in the *xy* plane at the beginning (a) and at the end (b) of the simulation. The important remarkable feature is that the molecule bilayers of PFL^- are interdigitated together during the 2 ns time of simulation, although the fluorocarbon chains of PFL^- are separated at the beginning, because of the strong hydrophobic interaction among them. Additionally, the fluorocarbon chains of PFL^- with a high rigidity are in the fluid state at room temperature, so the interdigitated form of bilayer lattice of linear hydrophobic chains are possible lamellar LLC phases maximizing packing and minimizing electrostatic repulsive interaction energy [33,44]. From the snapshot of the configuration at the end of the simulation, we can find that the counterions (Li^+) are adsorbent to the polar groups of the molecule bilayers, which can screen the electrostatic repulsion among the PFL^- headgroups. The detailed structural properties of the molecule bilayer and counterions (Li^+) in water system can be obtained by analyzing various radial distribution functions.

In Fig. 9a, the radial distribution functions $g_{ij}(r)$ are shown for Li^+ and headgroups, H_2O molecules, while Fig. 9b shows $g_{ij}(r)$ for oxygen atoms in carboxylic groups (Oc) and water oxygen atoms (Ow), Oc and H, F and H atoms. The $g_{Li^+\text{-}Oc}(r)$ can determine the thickness of the Stern layer [40,45,46]. The electrostatic attraction between negatively charged headgroups and Li^+ counterions leads to the well structured $g_{Li^+\text{-}Oc}(r)$, which has the first peak starting at 1.3 Å, and the second peak starting at 2.2 Å. The first peak represents the Stern layer, and its thickness is about 0.9 Å (1.3–2.2 Å). The second weaker peak is located at 2.5 Å, indicating that most of Li^+ counterions are located in the Stern layer at the same Helmholtz plane as the oxygen atoms in carboxylic groups (Oc), and a single Li^+ can be shared by several headgroups. Additionally, the strong hydration interaction between Li^+ and H_2O molecules makes $g_{Li^+\text{-}Oc}(r)$, and $g_{Li^+\text{-}H}(r)$, distribute similarly and well structured. This is because the volume of Li^+ is very small, leading to a high charging density. This is the predominant reason that the lithium perfluorofatty acids have lower Krafft points and can form LLC phases in aquous solutions with appropriate length of flourocarbon chains. In Fig. 8b, the first peak of $g_{Oc\text{-}H}(r)$ is also observed at the nearest distance (1.8 Å), due to the strong hydrogen bonding interaction between carboxylic groups and H_2O molecules. The $g_{Oc\text{-}H}(r)$ is completely consistent with the $g_{Oc\text{-}H}(r)$, so some of H_2O molecules can filter into the interspace among the headgroups. However, we cannot find any peaks in the curve of $g_{F\text{-}H}(r)$, indicating the fluorocarbon chains are highly hydrophobic, and so scarcely any H_2O molecules can filter into the highly hydrophobic bilayer of fluorocarbon chains.

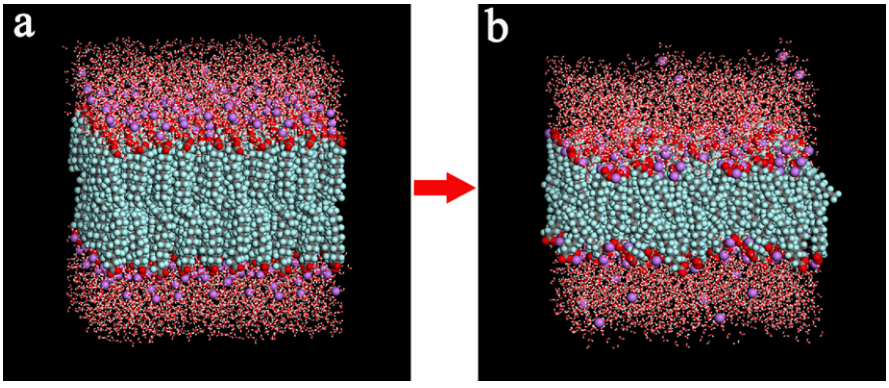

Fig. 8. Snapshots of the configuration of the system near the beginning (a) and at the end (b) of the simulation. The water molecules in both above and below sides are drawn as a line model, while surfactant molecules and lithium-ion are drawn as sphere and stick models, respectively.

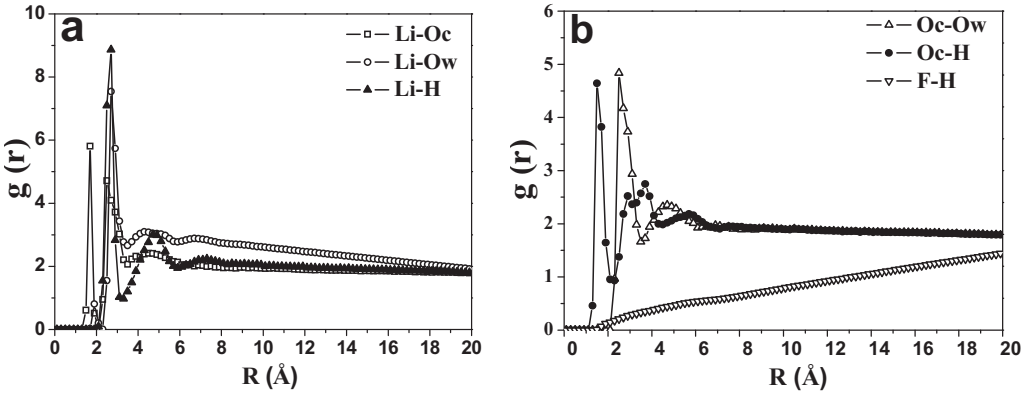

Fig. 9. Radial distribution functions of Li^+ ions and different atoms: Ow, Oc and H atoms (a); radial distribution functions of Oc and Ow, H atoms; F and H atoms (b). Oc denotes carboxylic group oxygen atoms, while Ow denotes water oxygen atoms.

3. Conclusions

In this article, we investigated the lyotropic liquid crystal (LLC) phases of lithium perfluorinated fatty acid salts (PFL/M-Li) in aqueous solutions. From our experimental results, we can find that the formation of lamellar LLC phases of perfluorofatty acid salts has some connection with their chain length and counterions, which is confirmed by NVT molecular dynamics simulation. Because the volume of Li^+ is very small, leading to much higher charging density. This is the predominant reason that the lithium perfluorofatty acid salts have lower Krafft points and can form LLC phases in aqueous solutions with appropriate length of fluorocarbon chains. Additionally, temperature and concentration of surfactant play an important role in the formation of LLC phases. With the increasing of chain lengths, the LLC-phase will become more temperature-resistable. From the results of MD simulation, one can observe that the molecule bilayers of PFL^- are interdigitated together, which is because the fluorocarbon chains of PFL^- with a high rigidity are in the fluid state at room temperature.

4. Experimental

4.1. Chemicals

Perfluorolauric acid (PFLA, 96%) was purchased from Matrix Scientific (Columbia, SC, USA), perfluorooctanoic acid (PFOA, 98%) and perfluorodecanoic acid (PFDA) perfluoromyristic acid (PFMA, 96%) were purchased from Fluorochem (Derbyshire SK13 7RY, UK). All the inorganic reagents such as lithium hydroxide (GR, 99%), sodium hydroxide (GR, 98%), potassium hydroxide (GR, 96%), caesium hydroxide (GR, 99%), etc. were purchased from Aladdin (Shanghai, China). Ultrapure water, with a resistivity of 18.25 MΩ cm, was obtained using a UPH-IV ultrapure water purifier (Chengdu Ultrapure Technology Co. Ltd., China).

4.2. Sample preparation

The corresponding perfluoroalkyl salts, PFO-Li, PFD-Li, PFL-Li, PFM-Li, PFL-Na, PFL-K, PFL-Cs, etc. samples were prepared by mixing equivalent amounts of perfluorinated fatty acids and relevant alkalis. The reactions were carried out with violently stirring at 70 °C for several hours. The solutions were placed into a vacuum extractor at -50.0 ± 0.1 °C for two days, and then white powder products were obtained. The perfluorinated fatty acid salts in water samples were prepared by mixing appropriate amounts of surfactants and water followed by stirring at about 70 °C until all the surfactants were dissolved. Then, all the samples were kept at 25.0 ± 0.1 °C for at least two weeks before their phase behavior was inspected and all the measurements were taken.

4.3. Characterizations

Differential scanning calorimetry (DSC) (DSC-Q10, TA instruments, USA) was used to determine the transition temperatures (T_c) of LLC-phases to micelle solutions. Samples were analyzed in aluminium pans under a flow of nitrogen (50 mL/min) and heated at 5 °C/min from 10 to 80 °C; an empty aluminium pan was used as a reference.

SAXS measurements were carried out at 298 K using a synchrotron radiation X-ray small-angle system on beamline 4B9A at the Beijing Synchrotron Radiation Facility (employed from Institute of High Energy Physics, Chinese Academy of Sciences). The imaging plate was a Mar345 with the resolution factor of 2048×2048. The two-dimensional SAXS scattering patterns consisted concentric circles, where the intensity (I) versus scattering vector (q) profile was independent of the azimuthal angle. A circular average of I was determined, to give the resulting I versus q plot. The range of scattering vectors was chosen from $q = 0.5$–$14\ nm^{-1}$ ($q = 4\pi/\lambda \sin\theta/2$, where θ and λ are the scattering angle and the incident X-ray wavelength of 1.38059 Å, respectively). The distance from a sample to a detector was 166 cm and the data accumulation time was 200 s for each sample.

The lamellar structure of the LLC phase was confirmed by FF-TEM for sample 400 mmol L^{-1} PFL-Li. A small amount of gel-like solution to be characterized was placed on a 0.1 mm thick coppor disk covered with a second copper disk. The copper sandwich with the sample was immersed rapidly into the liquid ethane cooled by liquid nitrogen. They were transferred into liquid nitrogen after several seconds. The samples, after being transferred into the chamber of the freeze-etching apparatus (Balzers BAF-400D), were fractured at a temperature and pressure of −150 °C and 10^{-7} Pa. After being etched for 1 min, Pt-C was sprayed onto the fracture face at 45°, and then C was sprayed at 90°. The replicas were examined on a JEOL 100CX-II TEM operating at an accerating voltage of 100 kV.

The rheological measurements were carried out with a Haake Rheostress 6000 rheometer using a Rotor C35/1 system at 25.0 ± 0.1 °C. The viscoelastic properties of the samples were determined by an oscillatory measurement from 0.01 to 100 Hz, and stress sweep measurements were made under with an oscillatory frequency of 1 Hz. In the investigation of thixotropy, a stepwise mode of shear rate was adopted. The shear rate was increased from 0.01 to 100 s^{-1} by 40 steps first, then held at 100 s^{-1} for 120 s, and then decreased to 0.01 by 40 steps.

Acknowledgements

This work was financially supported by the NSFC (Grant No. 21033005) and the National Basic Research Program of China (973 Program, 2009CB930103), and NFS of Shandong Province (2009ZRB01876).

Appendix A. Supplementary data

Supplementary data associated with this article can be found, in the online version, at doi:10.1016/j.jfluchem.2011.12.012.

References

[1] K. Shinoda, M. Hato, T. Hayashi, J. Phys. Chem. 76 (1972) 909–914.
[2] H. Kunieda, K. Shinoda, J. Phys. Chem. 80 (1972) 2468–2470.
[3] J. Israelachvili, D.J. Mitchell, B.W. Ninham, J. Chem Soc, J. Chem. Soc. Faraday Trans. 72 (1976) 1525–1568.
[4] K. Fontell, B. Lindman, J. Phys. Chem. 87 (1983) 3289–3297.
[5] R. Oda, I. Huc, D. Danino, Y. Talmon, Langmuir 16 (2000) 9759–9769.
[6] H. Hoffmann, J. Würtz, J. Mol. Liq. 72 (1997) 191–230.
[7] S.C. Sharma, R.G. Shrestha, L.K. Shrestha, K. Aramaki, J. Phys. Chem. B 113 (2009) 1615–1622.
[8] H. Hoffmann, J. Kalus, H. Thurn, Colloid. Polym. Sci. 261 (1983) 1043–1049.
[9] S. Dong, X. Li, G. Xu, H. Hoffmann, J. Phys. Chem. B 111 (2007) 5903–5910.
[10] T. Asakawa, H. Sunagawa, S. Miyagishi, Langmuir 14 (1998) 7091–7094.
[11] N. Boden, S.A. Corne, K.W. Jolley, J. Phys. Chem. 91 (1987) 4092–4105.
[12] M.C. Holmes, D.J. Reynolds, N. Boden, J. Phys. Chem. 91 (1987) 5257–5262.
[13] H. Iijima, T. Kato, H. Yoshida, M. Imai, J. Phys. Chem. B 102 (1998) 990–995.
[14] S.S. Berr, R.R.M. Jones, J. Phys. Chem. 93 (1989) 2555–2558.
[15] R. Muzzalupo, G.A. Ranieri, C. La Mesa, Colloid Surf. A 104 (1995) 327–336.
[16] J. Hao, H. Hoffmann, K. Horbaschek, Langmuir 17 (2001) 4151–4160.
[17] X. Li, S. Dong, X. Jia, A. Song, J. Hao, Chem. Eur. J. 13 (2007) 9495–9502.
[18] V.M. Sadtler, M.P. Krafft, J.G. Riess, Angew. Chem. Int. Ed. 35 (1996) 1976–1978.
[19] Y. Kondo, N. Yoshino, Curr. Opin. Colloid Interface Sci. 10 (2005) 88–93.
[20] K. Wang, G. Orädd, M. Almgren, T. Asakawa, B. Bergenståhl, Langmuir 16 (1999) 1042–1049.
[21] S. Mele, B.W. Ninham, M. Monduzzi, J. Phys. Chem. B 108 (2004) 17751–17759.
[22] G.J.T. Tiddy, B.A. Wheeler, J. Colloid Interface Sci. 47 (1974) 59–64.
[23] P. Kekicheff, G.J.T. Tiddy, J. Phys. Chem. 93 (1989) 2520–2526.
[24] M.H. Ropers, M.J. Stébé, Langmuir 19 (2003) 3137–3144.
[25] R.G. Shrestha, L.K. Shrestha, S.C. Sharma, K. Aramaki, J. Phys. Chem. B 112 (2008) 10520–10527.
[26] S. Bandyopadhyay, M. Tarek, M.L. Lynch, M.L. Klein, Langmuir 16 (2000) 942–946.
[27] R. Wu, M. Deng, B. Kong, X. Yang, J. Phys. Chem. B 113 (2009) 15010–15016.
[28] L. De Gaetani, G. Prampolini, Soft Matter 5 (2009) 3517–3526.
[29] A. Debnath, K.G. Ayappa, V. Kumaran, P.K. Maiti, J. Phys. Chem. B 113 (2009) 10660–10668.
[30] S. Balasubramanian, S. Pal, B. Bagchi, Curr. Sci. 82 (2002) 845–855.
[31] C. Vautrin, M. Dubois, Th. Zemb, St. Schmölzer, H. Hoffmann, M. Gradzielski, Colloids Surf. A 217 (2003) 165–170.
[32] J. Hao, H. Hoffmann, Curr. Opin. Colloid Interface Sci. 9 (2004) 279–293.
[33] T. Zemb, M. Dubois, Aust. J. Chem. 56 (2003) 971–979.
[34] P. Long, J. Hao, Soft Matter 6 (2010) 4350–4356.
[35] L. Herbst, H. Hoffmann, J. Kalus, K. Reizlein, U. Schmelzer, Ber. Bunsenges. Phys. Chem. 89 (1985) 1050–1064.
[36] R. Weber, H. Hoffmann, Liq. Cryst. 3 (1988) 203–216.
[37] R. Kumar, G.C. Kalur, L. Ziserman, D. Danino, S.R. Raghavan, Langmuir 23 (2007) 12849–12856.
[38] W. Jiang, J. Hao, Z. Wu, Langmuir 24 (2008) 3150–3156.
[39] S. Yuan, L. Ma, X. Zhang, L. Zheng, Colloids Surf. A 289 (2006) 1–9.
[40] T. Zhao, G. Xu, S. Yuan, Y. Chen, H. Yan, J. Phys. Chem. B 114 (2010) 5025–5033.
[41] H. Sun, P. Ren, J.R. Fried, Comput. Theor. Polym. Sci. 8 (1998) 229–246.
[42] H. Sun, J. Phys. Chem. B 102 (1998) 7338–7364.
[43] J. Chanda, S. Chakraborty, S. Bandyopadhyay, J. Phys. Chem. B 109 (2004) 471–479.
[44] M. Dubois, V. Lizunov, A. Meister, T. Gulik-Krzywicki, J.M. Verbavatz, E. Perez, J. Zimmerberg, T. Zemb, PNAS 101 (2004) 15082–15087.
[45] V.L. Shapovalov, M.E. Ryskin, O.V. Konovalov, A. Hermelink, G. Brezesinski, J. Phys. Chem. B 111 (2007) 3927–3934.
[46] Z. Hu, J. Jiang, Langmuir 24 (2008) 4215–4223.